Mechatronics 110 (2025) 103364

Contents lists available at ScienceDirect

Mechatronics

journal homepage: www.elsevier.com/locate/mechatronics

Practical and robust incremental model predictive control for flexible-joint robots☆

Yongchao Wang [a,c], Tian Zheng [b,c], Maged Iskandar [d], Marion Leibold [d], Jinoh Lee [d,e,*]

[a] School of Aerospace Science and Technology, Xidian University, South Taibai Road 2, Xi'an, 710071, China
[b] Chair of Traffic Engineering and Control, Technical University of Munich, Munich, 80333, Germany
[c] Chair of Automatic Control Engineering (LSR), Technical University of Munich, Munich, 80333, Germany
[d] Institute of Robotics and Mechatronics, German Aerospace Center (DLR), Weßling, 82234, Germany
[e] Department of Mechanical Engineering, KAIST, Daejeon, Republic of Korea

ARTICLE INFO

Keywords:
Flexible joint
Model predictive control
Time-delay estimation
Optimization-based control

ABSTRACT

This article proposes an optimization-based method for robust yet efficient control of flexible-joint robots by using the model predictive control approach. The time-delay estimation (TDE) technique is used to approximate uncertain and nonlinear dynamic equations, where neither concrete knowledge of mathematical system model parameters is required in the approximation, thus granting the model-free property for dynamics compensation and real-time system linearization. TDE is integrated with model predictive control, which is designated as the incremental model predictive control (IMPC) framework. This approach guarantees the tracking performance of the flexible joint robot with input and output constraints, such as motor torque and joint states. Moreover, the proposed controller can practically circumvent high-order derivatives in implementation while providing robust tracking, a capability that conventional methods for flexible joint robots often face challenges due to the inherent nature of their high-order dynamics. The input-to-state stability of IMPC in a local region around the reachable reference trajectory is theoretically proven, and the high approximation accuracy of the resulting incremental system is analyzed. Finally, a series of experiments is conducted on a flexible-joint robot to verify the practical effectiveness of IMPC, and superior performance in terms of high accuracy, high computational efficiency, and constraint admissibility is demonstrated.

1. Introduction

For complex task operations in a cluttered and unstructured environment, it is crucial for the robot to exhibit flexibility and safety in the shared workspace. Owing to the passive compliance in series elastic actuators, flexible-joint robots are physically safe [1]. The flexible joints have been also considered for humanoid robots, primarily to emulate human motion characteristics and address the inherent limitations of rigid-body robots in safety, energy efficiency and environmental adaptability. As shown in Fig. 1, joints of the humanoid robot arm are driven by series elastic actuators. Unlike conventional rigid-body robotic arms, flexible-joint robot incorporates elastic elements (e.g., springs, elastomers) in addition to actuation units (e.g., motors, pneumatic actuators). The elastic joint torque is transmitted between the inertia of the motor and the link via joint stiffness, and the elastic actuator can temporarily store kinetic energy and release it when required, effectively improving energy efficiency. Besides, elastic elements absorb shock energy, reducing impact forces during accidental collisions between the robotic arm and external objects (or humans), enhancing safety especially when the robot is needed to perform precise manipulation tasks under the condition with human co-workers. However, the elasticity between the motor and link sides introduces a challenge to a sufficient control precision level. Besides, to further guarantee safe collaboration between humans and robots, the coexistence of high control accuracy and constraint admissibility is of great importance. In addition, the unwanted oscillatory behavior is invoked when motor constraints are not addressed properly [2]. Accordingly, we aim to develop a controller to improve tracking accuracy and address input and state constraints simultaneously.

☆ This paper was supported in part by ITECH R&D programs of MOTIE/KEIT under Grant No. 20026194 and RS-2024-00441872, and in part by the National Natural Science Foundation of China under Grant No. 62303484.

* Corresponding author at: Institute of Robotics and Mechatronics, German Aerospace Center (DLR), Weßling, 82234, Germany.
E-mail addresses: yongchao.wang@tum.de (Y. Wang), jinoh.lee@dlr.de (J. Lee).

https://doi.org/10.1016/j.mechatronics.2025.103364
Received 30 December 2024; Received in revised form 2 May 2025; Accepted 1 June 2025
Available online 26 June 2025

Nomenclature

$\mathbb{R}, \mathbb{R}_{\geq 0}, \mathbb{R}_{>0}$	Real, non-negative, and positive sets.
$\mathbb{I}, \mathbb{I}_{>0}$	Integer, and positive integer sets.
$\mathbb{I}_{[a,b]}$	$\mathbb{I}_{[a,b]} = \{x \in \mathbb{I} : a \leq x \leq b\}$.
$\mathbf{I}, \mathbf{O}, \mathbf{0}$	Identity matrix, null matrix, and null vector.
$\mathrm{col}(\mathbf{x}_1, \mathbf{x}_2)$	Stack variable $\mathrm{col}(\mathbf{x}_1, \mathbf{x}_2) := [\mathbf{x}_1^\top, \mathbf{x}_2^\top]^\top$.
$\mathbf{Q} \succ 0$	Positive definite matrix $\mathbf{Q}$.
$\|\mathbf{x}\|$	Euclidean norm of vector/matrix $\mathbf{x}$.
$\|\mathbf{x}\|_\mathbf{Q}$	$\|\mathbf{x}\|_\mathbf{Q} = \sqrt{\mathbf{x}^\top \mathbf{Q} \mathbf{x}}$ for vector $\mathbf{x}$ and $\mathbf{Q} \succ 0$.
$\lambda(\mathbf{Q})$	Eigenvalue of $\mathbf{Q}$.
$\mathcal{K}_\infty$	Class Kappa infinity function.
$\mathrm{id}(\bullet)$	Identity function, i.e., $\mathrm{id}(x) = x$.

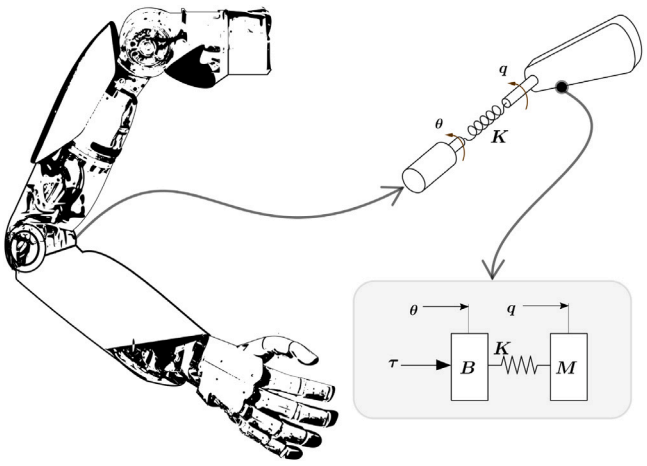

Fig. 1. Working mechanism of the flexible-joint robot.

1.1. Related work

Proportional–derivative (PD) feedback controllers [3,4] and backstepping (BS) [5] are early works to regulate and control the link position of flexible-joint robots, where full state variables and the concrete mathematical model are required. Although PD and BS are easy to implement, tracking accuracy deteriorates in the presence of inevitable uncertainties or disturbances.

To improve robustness, a variety of controllers like H_∞ control [6], sliding mode control [7,8], disturbance-observer-based control [9], neural-network (NN) based control [10], and adaptive fuzzy control [11] were developed. Although the mathematical model is not required for NN-based controllers, the application is still limited due to the requirement of offline training with a sufficiently large data set and numerous parameters to be tuned. The time-delay estimation (TDE) technique [12–14] was employed to approximate nonlinear system models of the robot, and an approximated system dynamics is found monitoring the most recent states and control inputs. The controller developed in [15] employed link inertia information with dynamics coupling terms to define TDE gains, and the terminal sliding mode control is utilized to enhance robustness and realize faster convergence. In general, these robust controllers increase tracking accuracy. However, high-order derivatives used in the above-mentioned controllers often result in a noisy response.

To reduce the order of the system dynamics, the singular perturbation (SP) method [16–18] was employed. Two-time scale controllers [17,18] were developed for flexible-joint robots, where the system dynamics is splitted into a slow and fast subsystem and control for both the slow and fast subsystems is designed independently. In [18], the tracking error is reduced by adding an additional perturbation term to the slow subsystem model of the flexible-joint robot. Nevertheless, the SP based controllers [17,18] and above-mentioned robust controllers [6–11,15] barely consider input and state constraints which are related to safety especially when the robot is close to or in cooperation with humans. Although using the command filter [19] or barrier function [20] techniques, the input saturation and state constraints can be addressed. Nevertheless, the command filter and barrier function normally employ conservative techniques to handle input and state constraints. As a result, the input and state constraints are addressed in sacrifice of tracking accuracy.

Model predictive control (MPC) [21,22] is appealing for control of flexible-joint robots since it is a systematic approach to achieve optimal control performance while satisfying input and state constraints. Motivated by the two-time-scales separation from the SP theory, a joint-level model predictive controller [22] was developed for flexible-joint robots. The conventional MPC approaches rely on a precise mathematical model of the controlled plant. As a result, tracking accuracy will be deteriorated by modeling errors [23]. To enhance the robustness of MPC, high-order extended observers [24], learning techniques [25,26], and data-driven methods [27] are combined with MPC, where mathematical models of controlled plants (or uncertainties and disturbances) are identified online and the accurate mathematical model is not required. However, the nominal mathematical model is still required for disturbance-observer-based MPC schemes. Although learning-based and data-driven MPC methods reduce dependence on the concrete mathematical model, the computational complexity of MPC is further aggravated by the learning and data-driven techniques. Therefore, a robust and computationally efficient MPC is required to achieve satisfactory performance in terms of high tracking accuracy and real-time control capability.

1.2. Method and contribution

In this article, an incremental model predictive controller is developed for flexible-joint robots. The dynamics equation of the flexible-joint robot is considered as a cascaded system, which involves two subsystems: dynamics equations on the link and motor sides. Each subsystem is firstly approximated by TDE, and incremental systems are obtained, where the torque due to the joint compliance is considered as an intermediate control variable. Then, the incremental model predictive control (IMPC) is developed through formulating a constrained optimal control problem (OCP) and physical constraints are considered. Finally, the effectiveness of the developed IMPC is verified by experiments on a flexible-joint robot. The main contributions of this article are summarized as follows:

(1) Improving Robustness and Computational Efficiency. TDE estimates the nonlinear dynamics without the use of model parameters and one can approximate the system dynamics as the discrete incremental system. Accordingly, if combined with a quadratic cost function to realize reference tracking, the constrained OCP is a quadratic program (QP), and it formulates IMPC, which is linear yet embodied with robustly approximated nonlinear dynamics, especially including uncertain and unmodeled dynamics. Compared with nonlinear MPC schemes which generally suffer from model parameter identification for complicated dynamics of the flexible joint robot system and its high computation cost, the proposed IMPC significantly improves the computational efficiency. In Section 5, a computationally efficient QP solver is employed and real-time experiments with 1 kHz control frequency are implemented.[1]

[1] We use `qpOASES` [28] as a baseline QP solver for the purpose of performance evaluation, while the computation speed can be further improved employing other state-of-the-art libraries known to be more efficient than `qpOASES`.

(2) Considering Physical Constraints. Due to the underactuated nature of the connected link and motor dynamics, it is challenging to guarantee satisfactory control performance while satisfying physical constraints related to safety, such as motor and state constraints on both the link and motor sides. Typically, the safety aspect of control is addressed at a higher level of the control loop with a slower sampling frequency, such as in the motion planner. This approach necessitates an immediate and inherent safety function to prevent violations of physical constraints (e.g., limits of actuator torque, joint angle, and speed) ensuring the protection of both the robot and its environment. This requirement is further emphasized for flexible robots due to their underactuated nature. In this article, by considering the joint compliance torque as the intermediate variable, we newly formulate IMPC for the resulting cascaded system dynamics. Physical constraints are incorporated as inequality constraints holistically in the fast low-level control loop to create the control torque. Notably, the IMPC method has never been formulated for controlling flexible-joint robots.

(3) Avoiding High-Order Derivatives. Control algorithms for flexible-joint robots typically require high-order derivatives, as evident in conventional feedback linearization-based methods [29,30] and more modern approaches such as elastic preserving structure control [31] and TDE-based methods [15]. To ensure optimal tracking, it is essential that the joint trajectories are sufficiently smooth, generally speaking, and posses at least fourth-order differentiability. Additionally, the feedback signals of the elastic joint should be differentiated at least three times, if not four. However, these high-order derivative signals are significantly influenced by measurement noises, necessitating the use of sensors with exceptionally high resolution and minimal noise. Nevertheless, oscillating responses at high frequencies are frequently observed, which can induce mechanical noises and reduce the lifespan of mechanical components of the robot. Accordingly, the proposed methodology is designed to calculate control signals by solving a constrained OCP, as an avenue of computation that circumvents the necessity for high-order derivatives, thereby mitigating the impact of noisy responses.

1.3. Organization

The rest of this article is organized as follows: In Section 2, the dynamics equation of the flexible-joint robot and the control objective are introduced. In Section 3, the incremental model predictive controller is developed through formulating a constrained OCP. Section 4 analyzes input-to-state stability. The effectiveness of the controller is verified in Section 5, where a series of experiments is conducted on a flexible-joint robot. Finally, Section 7 draws a conclusion.

2. Problem formulation

In this section, we first introduce the dynamics equation of the flexible-joint robot and then the control objective is given.

2.1. Flexible-joint robot dynamics

The dynamics of an n-DoF flexible-joint robot is modeled by the following equations:

$$\mathbf{M}(\mathbf{q})\ddot{\mathbf{q}} + \mathbf{C}(\mathbf{q},\dot{\mathbf{q}}) + \mathbf{G}(\mathbf{q}) + \mathbf{w}_{\mathrm{l}} = \boldsymbol{\Gamma}, \tag{1a}$$

$$\mathbf{D}\ddot{\boldsymbol{\theta}} + \mathbf{w}_{\mathrm{m}} + \boldsymbol{\Gamma} = \boldsymbol{\tau}, \tag{1b}$$

$$\boldsymbol{\Gamma} = \mathbf{K}(\boldsymbol{\theta} - \mathbf{q}), \tag{1c}$$

where $\mathbf{q}$, $\dot{\mathbf{q}}$, $\ddot{\mathbf{q}} \in \mathbb{R}^n$ represent joint positions, velocities, and accelerations, respectively. $\mathbf{M}(\mathbf{q}) \in \mathbb{R}^{n\times n}$ is the link inertia matrix, $\mathbf{C}(\mathbf{q},\dot{\mathbf{q}}) \in \mathbb{R}^n$ is Coriolis/centrifugal forces vector on the link side, $\mathbf{G}(\mathbf{q}) \in \mathbb{R}^n$ contains the gravitational terms exerting on the link side, $\mathbf{w}_{\mathrm{l}} \in \mathbb{R}^n$ represents the friction and disturbance forces in links, and $\boldsymbol{\Gamma} \in \mathbb{R}^n$ is the vector of torques due to the joint compliance specified in (1c), where $\mathbf{K} \in \mathbb{R}^{n\times n}$ is the diagonal joint stiffness matrix. In (1b), $\mathbf{D} \in \mathbb{R}^{n\times n}$ is the diagonal motor inertia matrix with rotors and gears, $\boldsymbol{\theta} \in \mathbb{R}^n$ is the motor position vector, $\boldsymbol{\tau} \in \mathbb{R}^n$ is the torque supplied by actuators on motors, and $\mathbf{w}_{\mathrm{m}} \in \mathbb{R}^n$ denotes friction and disturbance forces in motors.

Since modeling errors exist, dynamics functions, such as $\mathbf{M}(\mathbf{q})$, $\mathbf{D}$, $\mathbf{C}(\mathbf{q},\dot{\mathbf{q}})$, $\mathbf{w}_{\mathrm{l}}$, and $\mathbf{w}_{\mathrm{m}}$, are assumed to be unknown/uncertain. Besides, for flexible-joint robots, the following property is satisfied.

Property 1 (*Positive Definite Inertia Matrices*)**.** *The unknown link and motor inertia matrices* $\mathbf{M}(\mathbf{q})$ *and* $\mathbf{D}$ *are uniformly positive definite, i.e., there exist positive constants* m_1, m_2, n_1, *and* n_2, *such that each eigenvalue of* $\mathbf{M}(\mathbf{q})$ *and* $\mathbf{D}$, *denoted by* $\lambda_i(\mathbf{M}(\mathbf{q}))$ *and* $\lambda_i(\mathbf{D})$ *(*$i \in \mathbb{I}_{[1,n]}$*), satisfies* $m_1 \le \lambda_i(\mathbf{M}(\mathbf{q})) \le m_2$ *and* $n_1 \le \lambda_i(\mathbf{D}) \le n_2$ *[13,14].*

Note that parameters m_1, m_2, n_1, and n_2 in Property 1 are used to show that inertia matrices $\mathbf{M}(\mathbf{q})$ and $\mathbf{D}$ are uniformly positive definite, though their exact values are not required to design controllers. The existence of constants in Property 1 is the theoretical basis to determine controller parameters, especially TDE parameters $\bar{\mathbf{M}}$ and $\bar{\mathbf{D}}$, in Section 3.

2.2. Control objective

Our aim is to design a robust controller that makes the flexible-joint robot track a reference trajectory in joint space. Besides, to guarantee safety, physical constraints of the robot, such as joint positions, velocities, and torques, are not violated, i.e., the following constraints on states and inputs are imposed:

$$\left(\mathbf{q},\dot{\mathbf{q}},\boldsymbol{\theta},\dot{\boldsymbol{\theta}},\boldsymbol{\tau}\right) \in \mathbb{X}_1 \times \mathbb{X}_2 \times \mathbb{X}_3 \times \mathbb{X}_4 \times \mathbb{U}, \tag{2}$$

where $\mathbb{X}_i$ ($i \in \mathbb{I}_{[1,4]}$) and $\mathbb{U}$ are all compact sets containing the origin in their interior. In the context of our robot, the link/motor position, velocity, and acceleration constraints are specified as follows:

$$\mathbf{q}_{\min} \le \mathbf{q} \le \mathbf{q}_{\max},\ \dot{\mathbf{q}}_{\min} \le \dot{\mathbf{q}} \le \dot{\mathbf{q}}_{\max}, \tag{3a}$$

$$\boldsymbol{\theta}_{\min} \le \boldsymbol{\theta} \le \boldsymbol{\theta}_{\max},\ \dot{\boldsymbol{\theta}}_{\min} \le \dot{\boldsymbol{\theta}} \le \dot{\boldsymbol{\theta}}_{\max}, \tag{3b}$$

$$\boldsymbol{\tau}_{\min} \le \boldsymbol{\tau} \le \boldsymbol{\tau}_{\max}, \tag{3c}$$

where $\bullet_{\min}$ and $\bullet_{\max}$ are lower and upper bounds.

Before the controller design, we make the following assumption on the reference trajectory $\mathbf{q}_{\mathrm{d}}$.

Assumption 1 (*Smooth Reference Trajectories*)**.** There exists a constant $c_{\mathrm{b}} \in \mathbb{R}_{>0}$ such that the reference trajectory $\mathbf{q}_{\mathrm{d}}$ satisfies $\| \left[\mathbf{q}_{\mathrm{d}}, \dot{\mathbf{q}}_{\mathrm{d}}\right] \| \le c_{\mathrm{b}}$ [32].

In practice, Assumption 1 is reasonable, since non-smooth reference trajectories will pose a threat to the mechanical system due to sharp actuator changes.

3. Incremental model predictive control

In this section, the incremental model predictive controller for flexible-joint robots is developed. First, to address modeling errors and also eliminate the dependence on a specific mathematical model of the dynamics equation, the TDE technique is employed and incremental systems are obtained. Then, the approximation accuracy of the resulting incremental systems is analyzed. Finally, based on incremental systems, the controller is designed in the framework of MPC considering physical constraints.

3.1. Incremental systems

In this subsection, we first approximate the dynamics equation on the link side (1a) using TDE, which involves two steps [12–14,32,33].

Step 1: Separation. Introducing a TDE parameter $\bar{\mathbf{M}}$, the uncertain dynamics equation on the link side (1a) is divided into known and unknown parts.

$$\bar{\mathbf{M}}\ddot{\mathbf{q}} + \underbrace{\left(\mathbf{M}(\mathbf{q}) - \bar{\mathbf{M}}\right)\ddot{\mathbf{q}} + \mathbf{C}\left(\mathbf{q}, \dot{\mathbf{q}}\right) + \mathbf{G}(\mathbf{q}) + \mathbf{w}_{\mathrm{l}}}_{\mathbf{H}} = \boldsymbol{\Gamma}, \tag{4}$$

where $\mathbf{H}$ includes all unmodeled/uncertain dynamics terms.

Step 2: Approximation. The value of $\mathbf{H}$ at time t will be approximated by its value at time $(t - L)$:

$$\begin{aligned}\mathbf{H}_t \cong \mathbf{H}_{(t-L)} &\overset{(4)}{=} \boldsymbol{\Gamma}_{(t-L)} - \bar{\mathbf{M}}\ddot{\mathbf{q}}_{(t-L)} \\ &\overset{(1c)}{=} \mathbf{K}(\boldsymbol{\theta}_{(t-L)} - \mathbf{q}_{(t-L)}) - \bar{\mathbf{M}}\ddot{\mathbf{q}}_{(t-L)},\end{aligned} \tag{5}$$

where L is a delay time. Then, considering the joint compliance torque $\boldsymbol{\Gamma}$ as the intermediate control variable, the incremental dynamics equation on the link side is obtained by the combination of (4) and (5):

$$\ddot{\mathbf{q}} = \ddot{\mathbf{q}}_0 + \bar{\mathbf{M}}^{-1}\left(\mathbf{K}\left(\Delta\boldsymbol{\theta} - \Delta\mathbf{q}\right) + \boldsymbol{\varepsilon}_1\right), \tag{6}$$

where $\ddot{\mathbf{q}}_0 := \ddot{\mathbf{q}}_{(t-L)}$, $\Delta\boldsymbol{\theta} := \boldsymbol{\theta}_t - \boldsymbol{\theta}_{(t-L)}$ and $\Delta\mathbf{q} := \mathbf{q}_t - \mathbf{q}_{(t-L)}$ are incremental variables, and $\boldsymbol{\varepsilon}_1 := \mathbf{H}_t - \mathbf{H}_{(t-L)}$ is the TDE error of $\mathbf{H}$.

Similarly, with an TDE parameter $\bar{\mathbf{D}}$, the dynamics equation on the motor side (1b) is transformed into the following incremental form:

$$\ddot{\boldsymbol{\theta}} = \ddot{\boldsymbol{\theta}}_0 + \bar{\mathbf{D}}^{-1}\left(\Delta\boldsymbol{\tau} + \boldsymbol{\varepsilon}_2\right), \tag{7}$$

where $\ddot{\boldsymbol{\theta}}_0 := \ddot{\boldsymbol{\theta}}_{(t-L)}$, $\Delta\boldsymbol{\tau} := \boldsymbol{\tau}_t - \boldsymbol{\tau}_{(t-L)}$ is the incremental control variable, and $\boldsymbol{\varepsilon}_2$ is the TDE error of the lumped uncertain dynamics function on the motor side.

In summary, the dynamics equations both on link and motor sides are approximated using TDE, and a concrete mathematical model is not required. Merely, the most recent state measurements are used.

According to the formal TDE implementation [12–14,32,33], the sampling period T_{s} is selected as L, which guarantees the delay time is sufficiently small. In practice, a digital system is regarded as a continuous one when the sampling rate is faster than 30 times the system bandwidth [34]. Thus, in accordance with the continuity property, TDE errors $\boldsymbol{\varepsilon}_1$ and $\boldsymbol{\varepsilon}_2$ are negligible when we select a sufficiently small delay time L. For $\boldsymbol{\varepsilon}_1 = \mathbf{0}$ and $\boldsymbol{\varepsilon}_2 = \mathbf{0}$, the nominal incremental systems for the dynamics equation (1) are obtained:

$$\begin{cases}\ddot{\mathbf{q}} = \ddot{\mathbf{q}}_0 + \bar{\mathbf{M}}^{-1}\mathbf{K}\left(\Delta\boldsymbol{\theta} - \Delta\mathbf{q}\right), \\ \ddot{\boldsymbol{\theta}} = \ddot{\boldsymbol{\theta}}_0 + \bar{\mathbf{D}}^{-1}\Delta\boldsymbol{\tau}.\end{cases} \tag{8}$$

Now the incremental systems (8) are discretized using Euler method to produce a model that is suitable for MPC. Since the sampling period T_{s} is sufficiently small, the discretization error is ignored. Thus, we have

$$\mathbf{x}(k+1) = \mathbf{A}_1\mathbf{x}(k) + \mathbf{A}_2\mathbf{x}(k-1) + \mathbf{B}_1\Delta\mathbf{u}(k), \tag{9}$$

where $\mathbf{x} := \mathrm{col}\left(\mathbf{x}_1, \mathbf{x}_2, \mathbf{x}_3, \mathbf{x}_4\right) := \mathrm{col}\left(\mathbf{q}, \dot{\mathbf{q}}, \theta, \dot{\theta}\right)$, while

$$\mathbf{A}_1 := \begin{bmatrix}\mathbf{I} & T_{\mathrm{s}}\mathbf{I} & \mathbf{O} & \mathbf{O} \\ \mathbf{O} & 2\mathbf{I} - T_{\mathrm{s}}^2\bar{\mathbf{M}}^{-1}\mathbf{K} & \mathbf{O} & T_{\mathrm{s}}^2\bar{\mathbf{M}}^{-1}\mathbf{K} \\ \mathbf{O} & \mathbf{O} & \mathbf{I} & T_{\mathrm{s}}\mathbf{I} \\ \mathbf{O} & \mathbf{O} & \mathbf{O} & 2\mathbf{I}\end{bmatrix},$$

$$\mathbf{A}_2 := \begin{bmatrix}\mathbf{O} & \mathbf{O} & \mathbf{O} & \mathbf{O} \\ \mathbf{O} & -\mathbf{I} & \mathbf{O} & \mathbf{O} \\ \mathbf{O} & \mathbf{O} & \mathbf{O} & \mathbf{O} \\ \mathbf{O} & \mathbf{O} & \mathbf{O} & -\mathbf{I}\end{bmatrix}, \text{ and } \mathbf{B}_1 := \begin{bmatrix}\mathbf{O} \\ \mathbf{O} \\ \mathbf{O} \\ T_{\mathrm{s}}\bar{\mathbf{D}}^{-1}\end{bmatrix}.$$

Define a stack variable $\mathbf{X}(k) := \mathrm{col}\left(\mathbf{x}(k), \mathbf{x}(k-1)\right)$, and (9) is transformed into the following canonical linear system:

$$\mathbf{X}(k+1) = \mathbf{A}\mathbf{X}(k) + \mathbf{B}\Delta\mathbf{u}(k), \tag{10}$$

where $\mathbf{A} := \begin{bmatrix}\mathbf{A}_1 & \mathbf{A}_2 \\ \mathbf{I} & \mathbf{O}\end{bmatrix}$, $\mathbf{B} := \begin{bmatrix}\mathbf{B}_1 \\ \mathbf{O}\end{bmatrix}$. In the following model predictive controller, (10) will be used to generate state predictions during the prediction horizon.

Now, with the TDE parameters $\bar{\mathbf{M}}$ and $\bar{\mathbf{D}}$, a linear approximation for the dynamics equation of the flexible-joint robot manipulator through monitoring state measurements. How to select TDE parameters will be analyzed in Remark 1.

3.2. Analysis of approximation accuracy

In Section 3, the incremental system is derived that only uses the most recent state measurements. However, due to the inevitable TDE error, there is a discrepancy between the real nonlinear dynamics and its incremental approximation. In this section, we will show that the resulting incremental system is able to exhibit a higher approximation accuracy than a nominal system model.

In the sequel, we take the dynamics equation on the link side as an example to analyze the approximation accuracy of the incremental system through a comparative analysis with the nominal counterpart. If the nominal inertia matrix, Coriolis/centrifugal vector, gravitational vector, and friction vector, denoted by $\mathbf{M}_{\mathrm{n}}$, $\mathbf{C}_{\mathrm{n}}$, $\mathbf{G}_{\mathrm{n}}$, and $\mathbf{w}_{\mathrm{l,n}}$ respectively, are available, the following nominal system dynamics equation is constructed in accordance with (1a):

$$\ddot{\mathbf{q}}_{\mathrm{n}} = \mathbf{M}_{\mathrm{n}}^{-1}\left(-\mathbf{C}_{\mathrm{n}} - \mathbf{G}_{\mathrm{n}} + \mathbf{w}_{\mathrm{l,n}} + \boldsymbol{\Gamma}\right), \tag{11}$$

where $\mathbf{q}_{\mathrm{n}}$ is the approximation of the joint position for the nominal case. To obtain the system dynamics approximation error, we recall the system dynamics (1a) and rewrite it as follows:

$$\mathbf{M}_{\mathrm{n}}\ddot{\mathbf{q}} + \tilde{\mathbf{M}}\ddot{\mathbf{q}} + \mathbf{C} + \mathbf{G} + \mathbf{w}_{\mathrm{l}} = \boldsymbol{\Gamma}, \tag{12}$$

where $\tilde{\mathbf{M}} := \mathbf{M} - \mathbf{M}_{\mathrm{n}}$ is the modeling error of the inertia matrix $\mathbf{M}$. From (11) and (12), one has the system dynamics approximation error for the nominal case as $\boldsymbol{\gamma} := \ddot{\mathbf{q}}_{\mathrm{n}} - \ddot{\mathbf{q}}$, then

$$\boldsymbol{\gamma} = \mathbf{M}_{\mathrm{n}}^{-1}\left(\tilde{\mathbf{M}}\ddot{\mathbf{q}} + \tilde{\mathbf{C}} + \tilde{\mathbf{G}} + \tilde{\mathbf{w}}_{\mathrm{l}}\right), \tag{13}$$

where $\tilde{\mathbf{C}} := \mathbf{C} - \mathbf{C}_{\mathrm{n}}$, $\tilde{\mathbf{G}} := \mathbf{G} - \mathbf{G}_{\mathrm{n}}$ and $\tilde{\mathbf{w}}_{\mathrm{l}} := \mathbf{w}_{\mathrm{l}} - \mathbf{w}_{\mathrm{l,n}}$ are modeling errors of $\mathbf{C}$, $\mathbf{G}$ and $\mathbf{w}_{\mathrm{l}}$, respectively.

Next, the system dynamics approximation error of the incremental system is analyzed. From (6) and (8), one observes that the system dynamics approximation error, denoted by $\boldsymbol{\delta}$, is related with the TDE error $\boldsymbol{\varepsilon}_1$, i.e.,

$$\begin{aligned}\boldsymbol{\delta} = \bar{\mathbf{M}}^{-1}\boldsymbol{\varepsilon}_1 &= \mathbf{H}_t - \mathbf{H}_{(t-L)} \\ &= \bar{\mathbf{M}}^{-1}\left(\left(\mathbf{M} - \bar{\mathbf{M}}\right)\ddot{\mathbf{q}} - \left(\mathbf{M}_{(t-L)} - \bar{\mathbf{M}}\right)\ddot{\mathbf{q}}_{(t-L)} + \boldsymbol{\varepsilon}_{\mathrm{d}}\right),\end{aligned} \tag{14}$$

where $\boldsymbol{\varepsilon}_{\mathrm{d}} := \boldsymbol{\varepsilon}_{\mathrm{c}} + \boldsymbol{\varepsilon}_{\mathrm{g}} + \boldsymbol{\varepsilon}_{\mathrm{l}}$, $\boldsymbol{\varepsilon}_{\mathrm{c}}$, $\boldsymbol{\varepsilon}_{\mathrm{g}}$ and $\boldsymbol{\varepsilon}_{\mathrm{l}}$ are TDE errors of $\mathbf{C}$, $\mathbf{G}$ and $\mathbf{w}_{\mathrm{l}}$, respectively.

Comparing (13) and (14) delivers that the major difference between the system dynamics approximation errors of the incremental system and the nominal counterpart is the inertia modeling error. For the incremental system, the inertia modeling error is compensated effectively by its time-delay values if the sampling period is sufficiently small. However, for the nominal case, the inertia modeling error cannot be compensated. Besides, $\boldsymbol{\varepsilon}_{\mathrm{d}}$ can be sufficiently small when a sufficiently high sampling frequency is employed. Therefore, the incremental system exhibits a higher approximation accuracy when the sampling period is sufficiently small.

From the above-mentioned approximation analysis, one learns that the approximation accuracy is related with the sampling period. In addition, from the perspective of the considered function itself, the system approximation accuracy is also related with the system dynamics. When the system operates at high frequencies, the function values vary significantly during a short period and the continuity property is challenging to be guaranteed. Then, the TDE error increases. To guarantee satisfactory control performance, we will focus on addressing large TDE errors in our future work.

Remark 1 (*How to Select Parameters* $\bar{\mathbf{M}}$ *and* $\bar{\mathbf{D}}$)**.** In existing TDE-based controllers, the stability condition requires to be fulfilled. In the context of the flexible-joint robot manipulator, the following inequalities need to be guaranteed to avoid performance deterioration by inappropriate TDE parameters $\bar{\mathbf{M}}$ and $\bar{\mathbf{D}}$: $\|\mathbf{I}-\mathbf{M}^{-1}\bar{\mathbf{M}}\| \leq 1$ and $\|\mathbf{I}-\mathbf{D}^{-1}\bar{\mathbf{D}}\| \leq 1$. In the sequel, taking the inertia matrix $\mathbf{M}$ for example to analyze how to select the TDE parameter $\bar{\mathbf{M}}$. In accordance with Property 1, $\mathbf{M}$ is uniformly positive definite and $\lambda_i(\mathbf{M})$ is bounded. Suppose $\bar{M}_i$ is the diagonal element of $\bar{\mathbf{M}}$, then $\forall i \in \mathbb{I}_{[1,n]}$, $\left(1-\frac{\bar{M}_i}{\lambda_i}\right)$ is an eigenvalue of the matrix $\left(\mathbf{I}-\mathbf{M}^{-1}\bar{\mathbf{M}}\right)$. If $\left\|1-\frac{\bar{M}_i}{\lambda_i}\right\| < 1$, i.e., $\bar{M}_i$ satisfies $0 < \bar{M}_i < 2\lambda_i$, then $\|\mathbf{I}-\mathbf{M}^{-1}\bar{\mathbf{M}}\| \leq 1$ holds. It implies that the sufficient condition $\|\mathbf{I}-\mathbf{M}^{-1}\bar{\mathbf{M}}\| \leq 1$ is achieved by a small positive $\bar{M}_i$ although exact expressions and eigenvalues are unknown. From the nature of TDE, too small $\bar{\mathbf{M}}$ results in large TDE errors while too large $\bar{\mathbf{M}}$ causes noisy responses. Similar to Lee et al. [14], Jin et al. [13] and Wang et al. [12,32,33], in this article, the TDE parameter $\bar{\mathbf{M}}$ is tuned following the procedures: (1) begin with sufficiently small positive $\bar{M}_i$ to guarantee stability; (2) increase $\bar{M}_i$ until tracking performance is satisfactory or the closed-loop system almost exhibits a noisy response. In practice, a wide range of $\bar{\mathbf{M}}$ can be selected, since the inertial modeling error $\mathbf{M}-\bar{\mathbf{M}}$ will be compensated by time-delayed signal (cf. (14)).

Remark 2 (*Robustness Against Payload Variation*)**.** In practice, inertia matrix $\mathbf{M}(\mathbf{q})$ and $\mathbf{D}$ are subjected to uncertainties due to payload variations, which may affect the stability condition. In the following, we will take $\mathbf{M}(\mathbf{q})$ for example to analyze the stability condition still holds under payload variations [35]. For ease of discussion, let $\mathbf{M}^*(\mathbf{q})$ and $\mathbf{M}^\dagger(\mathbf{q})$ be the value of $\mathbf{M}(\mathbf{q})$, with and without payload, and λ_i^* and $\lambda_i^\dagger$ ($i \in \mathbb{I}_{[1,n]}$) be corresponding eigenvalues. Suppose that $\bar{\mathbf{M}}$ is designed under no payload condition and satisfies the stability condition. In accordance with Remark 1, $\bar{M}_i < 2\lambda_i^\dagger$ holds. Next, the question of interest is whether $\bar{M}_i$ designed for the no-load situation still guarantees the stability condition for the payload situation ($\bar{M}_i < 2\lambda_i^*$). The inertia matrix $\mathbf{M}^*(\mathbf{q})$ can be expressed as follows: $\mathbf{M}^*(\mathbf{q}) = \mathbf{M}^\dagger(\mathbf{q}) + \Delta\mathbf{M}(\mathbf{q})$, where $\Delta\mathbf{M}(\mathbf{q})$ is attributable to the payload and semi-positive definite in general. Thus, $\lambda_i^* \geq \lambda_i^\dagger$ and then the stability criterion ($\bar{M}_i < 2\lambda_i^\dagger \leq 2\lambda_i^*$) holds. Therefore, the TDE parameter selected under the no-load condition still guarantees the stability condition for the robot manipulator with payloads.

Remark 3 (*Sufficiently Small Sampling Periods*)**.** To guarantee high approximation accuracy of the incremental system, a sufficiently small sampling period is required. However, too high sampling frequencies aggravate the computational burden, and real-time control is challenging to be guaranteed. Unfortunately, there has been no systematic methods to determine the allowable sampling periods for TDE-based controllers so far. In [12–14,32,33], TDE methods have been demonstrated the high-accuracy approximation capability with sampling periods of 1 ms and 2 ms for robotics systems. Accordingly, the sampling period of the considered flexible-joint robot is chosen as 1 ms.

Remark 4 (*Robustness Against Stiffness Uncertainties*)**.** It is a general assumption that the stiffness matrix $\mathbf{K}$ is known in controllers for flexible-joint robot manipulators. In contrast, the developed IMPC has less dependencies on stiffness information. According to the dynamics (1a) and (1c), the dynamics equation on the link side is rewritten as the following form:

$$\mathbf{M}^*(\mathbf{q})+\mathbf{C}^*(\mathbf{q},\dot{\mathbf{q}})+\mathbf{G}^*(\mathbf{q})+\mathbf{w}_l^* = \boldsymbol{\theta}-\mathbf{q},$$

where $\mathbf{M}^*(\mathbf{q}) := \mathbf{M}(\mathbf{q})\mathbf{K}^{-1}$, $\mathbf{C}^*(\mathbf{q},\dot{\mathbf{q}}) = \mathbf{C}(\mathbf{q},\dot{\mathbf{q}})\mathbf{K}^{-1}$, $\mathbf{G}^*(\mathbf{q}) = \mathbf{G}(\mathbf{q})\mathbf{K}^{-1}$, and $\mathbf{w}_l^* = \mathbf{w}_l\mathbf{K}^{-1}$. In accordance with Section 2 of the article, we obtain the approximation error of the incremental system as follows:

$$\boldsymbol{\delta}' = \bar{\mathbf{M}}^*\left[\left(\mathbf{M}^*-\bar{\mathbf{M}}^*\right)\ddot{\mathbf{q}} - \left(\mathbf{M}^*_{(t-L)}-\bar{\mathbf{M}}^*\right)\ddot{\mathbf{q}}_{(t-L)} + \boldsymbol{\varepsilon}_d'\right]$$

where $\bar{\mathbf{M}}^* = \bar{\mathbf{M}}\mathbf{K}_\mathrm{n}$, $\mathbf{K}_\mathrm{n}$ is the nominal value of $\mathbf{K}$. One also observes that the stiffness and inertia modeling error will be compensated by its time-delayed values, and robustness against stiffness uncertainties is enhanced.

3.3. Controller design

In this subsection, the incremental model predictive controller will be proposed. We formulate a constrained optimal control problem (OCP) using the developed linear incremental system (10). The control structure and signal flow in the real-time control loop are summarized in Fig. 2.

First, the stage cost function is defined. In accordance with the control aim and considering control efficiency, the tracking error and control signal are considered as ingredients of the stage cost function. Considering the reference trajectory is predefined, we define the stage cost function as follows:

$$\mathcal{L}(\mathbf{X}_{k+i+1|k}, \Delta\mathbf{u}_{k+i|k}, k) = \|\mathbf{E}_{k+i+1|k}\|_{\mathbf{Q}}^2 + \|\Delta\mathbf{u}_{k+i|k}\|_{\mathbf{R}}^2, \tag{15}$$

where $\mathbf{E}_{k+i+1|k} := \mathbf{S}\mathbf{X}_{k+i+1|k} - \mathbf{q}_\mathrm{d}(k+i+1)$, $\mathbf{S} := [\mathbf{I}\ \mathbf{O}\ \mathbf{O}\ \mathbf{O}]$, $\mathbf{Q} \succ 0$ and $\mathbf{R} \succ 0$ are weighting matrices, and $\bullet_{k+i|k}$ denotes predictions of states and control inputs, in particular, $\mathbf{X}_{k|k} := \mathbf{X}(k)$. The predictions are generated by the linear incremental system (10), i.e.,

$$\mathbf{X}_{k+i+1|k} = \mathbf{A}\mathbf{X}_{k+i|k} + \mathbf{B}\Delta\mathbf{u}_{k+i|k}, \tag{16}$$

with $i \in \mathbb{I}$ being an intermediate variable.

Then, based on the stage cost function (15), the incremental model predictive controller is developed through formulating a constrained OCP. In this paper, the following constrained OCP with a feasible control sequence $\Delta\bar{\mathbf{u}}_k := [\Delta\mathbf{u}_{k|k}, \dots, \Delta\mathbf{u}_{k+N-1|k}]$ is constructed:

$$\Delta\bar{\mathbf{u}}^* = \arg\min_{\Delta\bar{\mathbf{u}}_k} \sum_{i=0}^{N-1} \mathcal{L}(\mathbf{X}_{k+i+1|k}, \Delta\mathbf{u}_{k+i|k}, k) \tag{17a}$$

$$\text{s.t.}\quad \mathbf{X}_{k+i+1|k} = \mathbf{A}\mathbf{X}_{k+i|k} + \mathbf{B}\Delta\boldsymbol{u}_{k+i|k}, \tag{17b}$$

$$\mathbf{q}_{k+i+1|k} \in \mathbb{X}_1, \dot{\mathbf{q}}_{k+i+1|k} \in \mathbb{X}_2, \tag{17c}$$

$$\boldsymbol{\theta}_{k+i+1|k} \in \mathbb{X}_3, \dot{\boldsymbol{\theta}}_{k+i+1|k} \in \mathbb{X}_4, \tag{17d}$$

$$\boldsymbol{\tau}(k) + \sum_{j=0}^{i} \Delta\boldsymbol{\tau}_{k+j|k} \in \mathbb{U}, \tag{17e}$$

where $N \in \mathbb{I}_{>0}$ is the prediction horizon, $i \in \mathbb{I}_{[0,N-1]}$ and $j \in \mathbb{I}_{[0,i]}$ are intermediate variables. The equality constraint (17b) is used to generate state predictions during the prediction horizon while inequality constraints (17c)–(17e) are employed to impose constraints on the motor and link sides. $\Delta\bar{\mathbf{u}}^* := [\Delta\mathbf{u}^*_{k|k}, \dots, \Delta\mathbf{u}^*_{k+N-1|k}]$ is the optimal control sequence. The first column of the optimal control sequence $\Delta\bar{\mathbf{u}}^*$, denoted by $\Delta\mathbf{u}^*_{k|k}$, is applied to the system combined with the current control law $\mathbf{u}(k)$, i.e., $\mathbf{u}^*(k+1) = \mathbf{u}(k) + \Delta\bar{\mathbf{u}}^*_{k|k}$.

Note that when the flexible-joint robot manipulator in the configuration affected by gravity, theoretically the developed IMPC still works and the initial torque to maintain its configuration is required to be calculated. Although there will be modeling errors, the gravity modeling error will be compensated using the TDE technique.

Remark 5 (*QP*)**.** After using the TDE technique, the nonlinear dynamics equation (1) is approximated by the linear incremental system (10). In addition, the stage cost function (15) is convex and imposed constraints (17b)–(17e) are all linear. As a result, the constrained OCP (17) can be cast to a QP. Thus, the solution to the constrained OCP (17) exists and is unique, and computationally efficient QP solvers, such as qpOASES [28], can be employed to realize real-time control for controlled plants with high control frequencies.

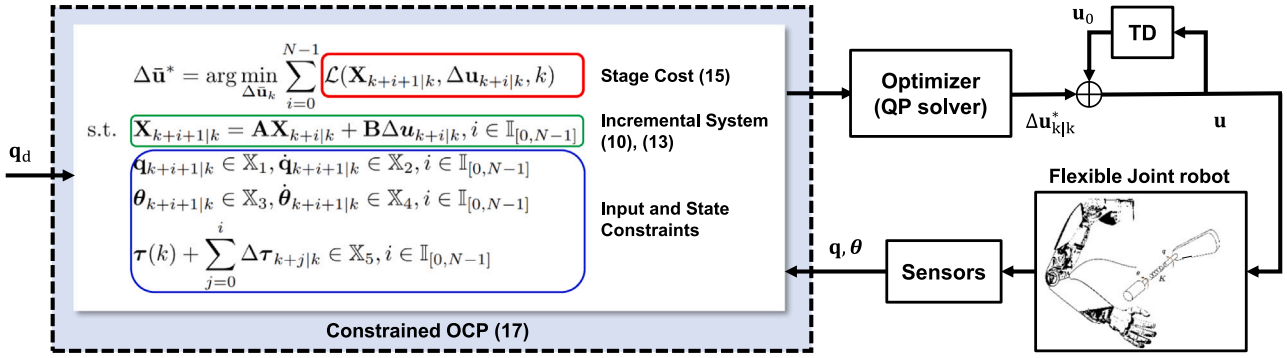

Fig. 2. The real-time control structure and signal flow of the developed incremental MPC, where "TD" denotes time delay of one sampling period.

Remark 6 (*Weighting Set Independent of Reference Signals*)**.** If, as an alternative, the controller law $\mathbf{u}$ is considered, and the stage cost function is designed: $\mathcal{L}(\mathbf{X}_{k+i+1|k}, \Delta\mathbf{u}_{k+i|k}, k) = \|\mathbf{E}_{k+i+1|k}\|^2_{\mathbf{Q}} + \|\mathbf{u}_{k+i|k}\|^2_{\mathbf{R}}$. However, $\mathbf{u}$ is not always equal to zero even the system is in equilibrium, since nonzero $\mathbf{u}$ is required to maintain the configuration and compensate for gravity. To guarantee tracking accuracy, we need to scale the term $\|\mathbf{u}_{k+j|k}\|^2_{\mathbf{R}}$ to be roughly the same size to the tracking error term $\|\mathbf{E}_{k+j|k}\|^2_{\mathbf{Q}}$. Thus, $\mathbf{R}$ should be tuned manually according to the target trajectory [36], and $\mathbf{R}$ should be readjusted when the reference trajectory changes. For a standard tracking MPC, the stage cost function (see Eq. (7) in [23]) involves the difference between the control signal and the reference counterpart, and the difference lies inside a small neighborhood around the origin for any reference signal. Thus, $\mathbf{R}$ can be determined without considering reference signals. Unfortunately, for the flexible-joint robot manipulator the reference control signal is not determined priorly. In this article, the stage cost function designed for the incremental MPC (cf. (15)) is similar to the standard stage cost for the tracking control scheme where the most recent control signal $\boldsymbol{\tau}_0$ is considered as the reference counterpart. Therefore, $\mathbf{R}$ can be determined without considering reference trajectories, owing to the incremental control structure.

4. Input-to-state stability analysis

In Section 3, the incremental MPC is developed where the TDE technique is used to approximate the uncertain dynamics equation. However, the TDE error is inevitable and stability will be affected by this error. Thus, stability will be investigated in the input-to-state stability (ISS) framework. In this section, ISS of the developed incremental MPC for the flexible-joint robot is demonstrated in a local region around one reachable reference trajectory. First, the definition of the reachable reference trajectory is given.

Definition 1 (*Reachable Reference Trajectory*)**.** The reference trajectory $\mathbf{q}_d$ is reachable if $\mathbf{q}_d$, $\dot{\mathbf{q}}_d$, the corresponding motor position $\boldsymbol{\theta}_c$, motor velocity $\dot{\boldsymbol{\theta}}_c$, and the controller $\mathbf{u}_c$ lie in tightened constraint sets $\bar{\mathbb{X}}_1$, $\bar{\mathbb{X}}_2$, $\bar{\mathbb{X}}_3$, $\bar{\mathbb{X}}_4$, and $\bar{\mathbb{U}}$, respectively, where $\bar{\mathbb{X}} \oplus \mathbb{C}^n_s \subseteq \mathbb{X}$, $\bar{\mathbb{U}} \oplus \mathbb{C}^n_r \subseteq \mathbb{U}$, $\bar{\mathbb{X}} := \bar{\mathbb{X}}_1 \times \bar{\mathbb{X}}_2 \times \bar{\mathbb{X}}_3 \times \bar{\mathbb{X}}_4$, s and r are positive scalars, $\mathbb{C} \subseteq \mathbb{R}^n := \{\mathbf{c} \in \mathbb{R}^n : -s\mathbf{1} \le \mathbf{c} \le s\mathbf{1}\}$, and $\oplus$ is the Minikowski sum.

According to *Definition 1* and *Lemma 4* in [32], we obtain that there exists a constant $V_{\max} \in \mathbb{R}_{>0}$ such that the optimal solutions from $\mathbf{X}(k)$ ($\mathbf{X}(k) \in \mathbb{D}$, $\mathbb{D} := \{\mathbf{X}(k), V_N(\mathbf{X}(k), k) \le V_{\max}\}$) also satisfy $\mathbf{X}^*_{k+j|k} \in \bar{\mathbb{X}}'$ and $\mathbf{u}^*_{k+j-1|k} \in \bar{\mathbb{U}}'$ for all immediate variable $j \in \mathbb{I}_{[1,N]}$, where $V_N(\mathbf{X}(k), k) := \min_{\Delta\bar{\mathbf{u}}_k} \sum_{j=0}^{N-1} \mathcal{L}(\mathbf{X}_{k+j+1|k}, \Delta\mathbf{u}_{k+j|k}, k)$ (s.t. constraints (17b)–(17e)) is the value function, both $\bar{\mathbb{X}}'$ and $\bar{\mathbb{U}}'$ are tightened constraint sets, $\bar{\mathbb{X}}' \oplus \mathbb{C}^n_{s'} \subseteq \mathbb{X}$, $\bar{\mathbb{U}}' \oplus \mathbb{C}^n_{r'} \subseteq \mathbb{U}$, s' and r' are positive scalars. Definition 1 implies that the reachable reference trajectory can be tracked and lies strictly in the tightened constraint set.

Next, we will demonstrate ISS of the developed incremental MPC in the following Theorem 1, where the main work in the proof is to analyze the regionally decreasing property of the value function $V_N(\mathbf{X}(k), k)$.

Theorem 1 (*Input-to-State Stability*)**.** *The developed IMPC admits ISS in a local region around one reachable reference trajectory for a large enough prediction horizon.*

Proof. According to ISS analysis in [23,32], $V_N(\mathbf{X}^*_{k+1|k}, k+1)$ is chosen as an auxiliary value function to avoid an overestimated cumulative error bound, and for a large enough but not infinite prediction horizon N, one has

$$V_N(\mathbf{X}^*_{k+1|k}, k+1) \le V_N(\mathbf{X}(k), k) - \alpha_V(V_N(\mathbf{X}(k), k)), \tag{18}$$

where $\alpha_V \in \mathcal{K}_\infty$, $\alpha_V(\bullet) \le \mathrm{id}(\bullet)$. According to *Lemma 3* in [32], for a sufficiently small sampling period, the TDE error is bounded. Thus, in accordance with (6)–(8), there exists a constant $\bar{\varepsilon} \in \mathbb{R}_{>0}$ such that

$$\|\mathbf{X}(k+1) - \mathbf{X}^*_{K+1|k}\| \le \|\boldsymbol{\varepsilon}\| \le \bar{\varepsilon}, \tag{19}$$

where $\boldsymbol{\varepsilon} := \mathrm{col}\left(\mathbf{0}, \bar{\mathbf{M}}^{-1}\boldsymbol{\varepsilon}_1, \mathbf{0}, \bar{\mathbf{D}}^{-1}\boldsymbol{\varepsilon}_2\right)$, composite TDE error.

Then, according to the Lipschitz continuity property of the value function (cf. *Lemma 5* in [32]), there exists a constant K_L such that

$$V_N(\mathbf{X}(k+1), k+1) - V_N(\mathbf{X}^*_{k+1|k}, k+1) \le K_L\bar{\varepsilon}. \tag{20}$$

Substituting (20) into (19) yields

$$\begin{aligned} &V_N(\mathbf{X}(k+1), k+1) - V_N(\mathbf{X}(k), k) \\ &\quad \le -\alpha_V(V_N(\mathbf{X}(k), k)) + K_L\bar{\varepsilon}. \end{aligned} \tag{21}$$

Thus, as shown in (21), the value function is regionally decreasing, i.e., $V_N(\mathbf{X}(k), k)$ is an ISS Lyapunov function.

In addition, based on the regionally decreasing property of $V_N(\mathbf{X}(k), k)$, recursive feasibility of the developed incremental MPC is analyzed. Assuming the TDE error is sufficiently small ($\bar{\varepsilon} \le \alpha_V(V_{\max})/K_L$) and $\mathbf{X}(k) \in \mathbb{D}$, one has

$$\begin{aligned} V_N(\mathbf{X}(k+1), k+1) &\le (\mathrm{id} - \alpha_V)\left(V_N(\mathbf{X}(k), k)\right) + K_L\bar{\varepsilon} \\ &\le (\mathrm{id} - \alpha_V)V_{\max} + \alpha_V(V_{\max}) \\ &\le V_{\max}. \end{aligned} \tag{22}$$

In accordance with (22), one learns that if $\mathbf{X}(k) \in \mathbb{D}$, then $\mathbf{X}(k+1) \in \mathbb{D}$. Using induction, it is shown that $V_N(\mathbf{X}(k+j), k+j) \le V_{\max}$ for all $j \in \mathbb{I}_{>0}$. Therefore, $\mathbb{D}$ is a positive invariant set, and $V_N(\mathbf{X}(k), k) \le V_{\max}$ holds recursively. The proof is completed.

In conclusion, the developed incremental MPC admits ISS in a local region $\mathbb{D}$ around reachable reference trajectories.

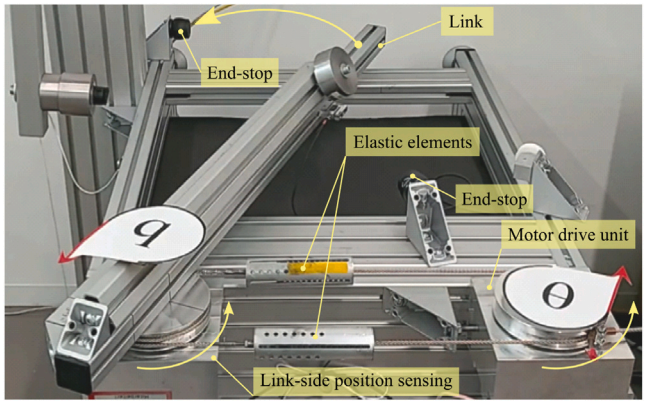

Fig. 3. Experimental setup of the flexible-joint robot testbed, called DLR Softy.

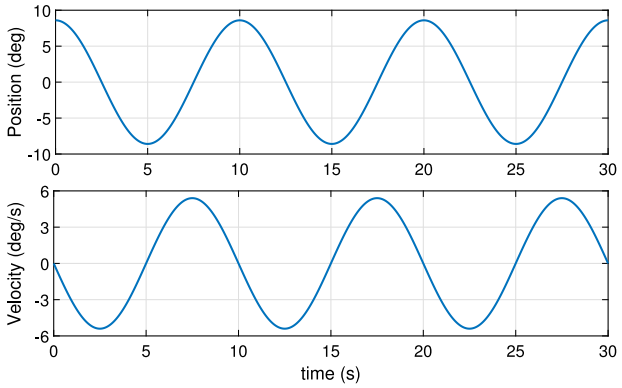

Fig. 4. Reference Signals for experiments.

Remark 7 (*How to Determine Prediction Horizons*)**.** In accordance with the theoretical analysis in Theorem 1 and results in [23,32], a large prediction horizon is essential to guarantee recursive feasibility of MPC without terminal ingredients. The tracking error decreases and the region of attraction enlarges with the rise of the prediction horizon. However, the methods to determine the minimal prediction horizon introduced in [23,32] are conservative, where the derived minimal prediction horizon is too large to realize real-time control. In practice, the prediction horizon is selected as large as possible to receive satisfactory control performance on the premise of ensuring real-time control.

Remark 8 (*Differentiation from the Previous Work*)**.** The main difference is originated from the system dynamics. Due to the spring component in the flexible-joint robot manipulator, the system dynamics of the flexible-joint robot manipulator is more complex than that of the rigid-body robot manipulator. Different from the TDE technique in our previous work [32], we consider the system dynamics of the flexible-joint robot manipulator as a cascaded system, and the system dynamics is divided into subsystems on both link and motor sides. Then, the TDE technique is employed to estimate these two subsystems, where the vector of torques due to the joint compliance is considered an intermediate control variable. As a result, the incremental version of the system dynamics modeled for the flexible-joint robot manipulator is obtained. Besides, this paper emphasizes avoiding high-order derivatives in controller design. This is a key practical advantages for the flexible-joint robot manipulator which is sensitive to measurement noises (see Fig. 3).

5. Experiments

To verify the effectiveness of the proposed controller, a series of experiments on a flexible-joint robot is conducted. The performance in terms of high accuracy, optimality, and constraint admissibility is demonstrated.

5.1. Experimental setup

The flexible-joint testbed, called Softy (cf. Fig. 3), is used for experimental validation, which is drove by a DLR Light Weight Robot (LWR) III drive unit [37] equipped with serial elastic components from the DLR C-runner robot [38]. For DLR Softy, the link position $\mathbf{q}$ and the motor position $\boldsymbol{\theta}$ are measured directly, while velocities and accelerations of link and motor sides are obtained by first-order numerical differentiation from the position measurement.

For the considered flexible-joint robot, controllers are computed with the sampling period of $T_s = 1$ ms, and the intrinsic joint stiffness is 362 N m/rad [39]. Parameters chosen for the proposed IMPC are listed as follows: control parameters $\bar{M} = 0.02$ and $\bar{D} = 0.012$, weighting matrix $\mathbf{Q} = \mathrm{diag}\{3000, 400, 300, 40\}$, $R = 1$, and the prediction horizon $N = 10$. The constrained OCP (17) is solved by the active-set QP solver, `qpOASES` [28]. In this article, two scenarios are considered in experiments. For both, the reference is sinusoidal with amplitude 0.15 rad and frequency 0.2π Hz (cf. Fig. 4).

5.2. Scenario 1 (S1): High accuracy, optimality, and high computational efficiency

5.2.1. Setting

To verify high accuracy and optimality of the developed incremental MPC, comparison experiments with PD controller for the flexible-joint robot [4] and time-delay sliding mode control (TDSMC) [15] are conducted. For simplicity, they are referred to as PD, TDSMC and IMPC, respectively. For the motor PD controller, $k_\mathrm{P} = 180$ and $k_\mathrm{D} = 80$, while for TDSMC, TDE parameters are the same as IMPC and the design parameters $k'_\mathrm{P} = 100$ and $k'_\mathrm{D} = 20$. For IMPC, the link/motor position, velocity, and torque limits are 20 deg, 20 deg/s, and 20 N m, respectively. The performance in terms of high accuracy and optimality is evaluated by investigating tracking errors and control signals. To quantitatively measure optimality, we use the following equation to calculate average cost C during a period $[0, t_s]$ with the stage cost function.

$$C = \frac{1}{N_t}\sum_{k=0}^{N_t}\left(\|\mathbf{e}(\mathbf{x}_i(k))\|^2_{\mathbf{Q}} + \|\Delta\boldsymbol{\tau}(k)\|^2_{\mathbf{R}}\right) \tag{23}$$

where $N_t = \frac{t_s}{T_s}$. In addition, computational efficiency of IMPC is investigated by its computing time at each iteration. Besides, to investigate effects of TDE parameters on tracking accuracy, experiments are implemented with TDE parameters $\bar{M} = 0.02, 0.005, 0.0025$.

5.2.2. Results

The experimental results are shown in Figs. 5–6. The root mean square errors (RMSE) of the Joint position tracking are shown in Table 1. PD controller, a model-based approach, presents the highest error among three controllers, while those are 3.1×10^{-2} deg for TDSMC and 6.0×10^{-2} deg for the proposed IMPC, respectively. While the tracking accuracy of TDSMC is highest among these three controllers, the developed incremental MPC still exhibits superior performance in terms of optimality and one can observe that the torque response generated by IMPC is much smoother than that of TDSMC as displayed in Fig. 6. This is due to the fact that in TDSCM, TDE and terminal sliding mode control are combined with the sole objective of reducing tracking errors using high-order derivatives of joint positions to calculate control torques. In contrast, the proposed IMPC takes into account not only the tracking precision but also the control efficiency as seen in the constrained OCP (17). Furthermore, high-order derivatives of joint positions are not

Table 1
Root-mean-square errors of different controllers (deg).

	PD	TDSMC	IMPC
RMSR	7.9×10^{-1}	3.1×10^{-2}	6.0×10^{-2}

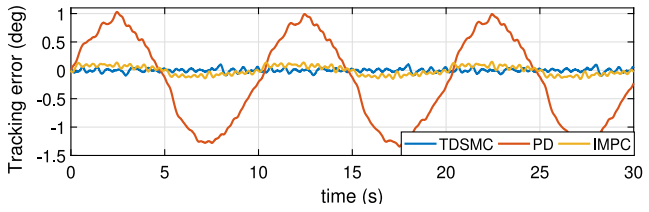

Fig. 5. Exp. results of *S1*: tracking errors of TDSMC, PD, and IMPC.

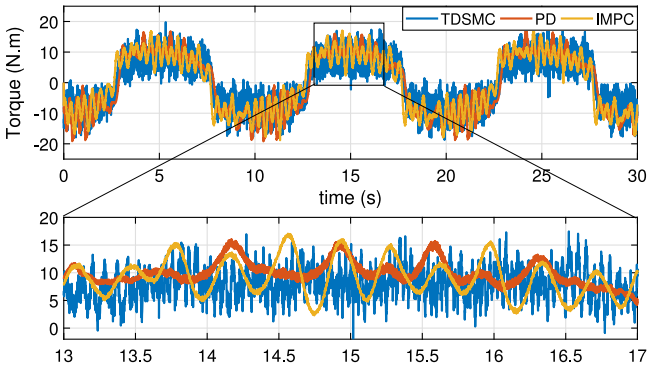

Fig. 6. Exp. results of *S1*: Control signals of TDSMC, PD, and IMPC.

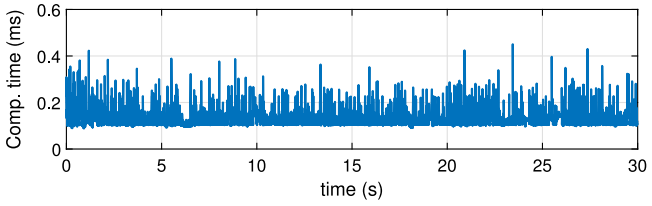

Fig. 7. Exp. results of *S1*: Computing time of IMPC at each iteration.

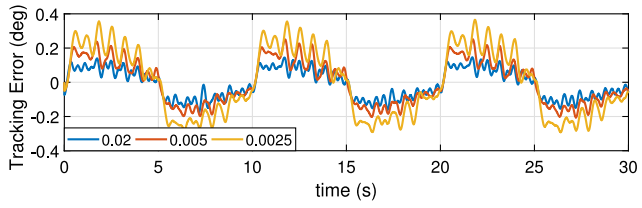

Fig. 8. Exp. results of *S2*: Tracking performance of IMPC with different TDE parameters.

required in IMPC, which results in a less noisy response. In accordance with (23), the average cost of PD, TDSMC, and IMPC are 1868.0, 26.1, and 11.2, respectively. The developed IMPC receives the same degree of control accuracy to TDSMC, while the average cost is much less than that of TDSMC. It verifies optimality of the developed IMPC quantitatively.

In Fig. 7, one observes that the computing time of IMPC at each iteration is less than one sampling period, 1 ms. It verifies the real-time control capability of IMPC in practice.

In Fig. 8, one learns that a wide range of TDE parameters can be selected and satisfactory tracking performance can be received. This is mainly due to the fact that the inertia modeling error can be

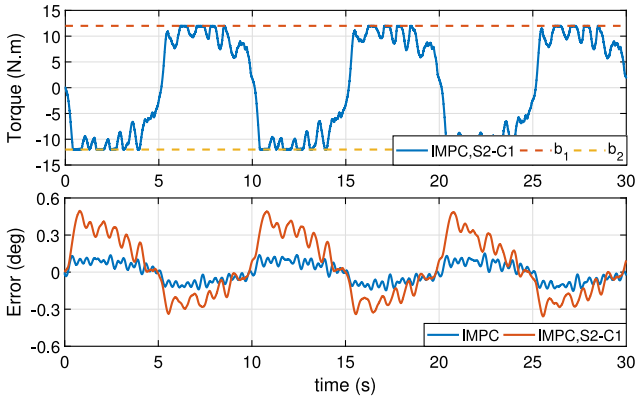

Fig. 9. Exp. results of *S2*: Tracking the performance of IMPC with tightened torque constraint, where "b_1" and "b_2" denote the lower and upper bound of torques, and "S2-C1" means Case 1 (C1) in S2.

compensated by its delayed values. Besides, one also observes that with the rise of the TDE parameter, the tacking error decreases. Thus, in practice, we can start with a small TDE parameter and increase until the system exhibits noisy responses.

5.3. Scenario 2 (S2): Constraint admissibility

5.3.1. Setting

In this scenario, we will impose tightened input and state constraints to check constraint admissibility of the developed IMPC. Two cases are considered with distinct limit values of input and output state constraints, as follows: position, velocity, and input torque, in that order, are given as

- Case 1 (C1): 20 deg, 20 deg/s, and 12 N m,
- Case 2 (C2): 20 deg, 4 deg/s, and 20 N m.

5.3.2. Results

The experimental results of C1 are shown in Fig. 9, where one can observe the input constraint is not violated. The system is stable and oscillation phenomenon is attenuated when input saturation occurs. Due to the limited torque, tracking errors are larger than that in *Scenario 1*.

The experimental results of C2 are shown in Fig. 10. From Fig. 10, we learn that on the whole, the joint velocity constraints are satisfied. However, due to ignorance of the TDE error and measurement resolution in the developed IMPC, there exist state prediction errors. As a result, the state constraints are slightly violated. During real-time experiments, we observe that the velocity constraint is challenging to be guaranteed, mainly, because the joint velocity is calculated using the numerical method. Although the state constraint violation phenomenon occurs slightly around the constraint boundary, the proposed IMPC still has the capability to regulate states to a large extent and the closed-loop system is still stable.

6. Numerical simulations

The effectiveness of HIMPC is now in addition validated by simulations for a 2-DoF flexible-joint robot manipulator.

6.1. Simulation setup

We simulate on a 2-DoF flexible-joint robot manipulator in [40], where the electric dynamics of the motor is ignored to keep consistent with this article. The detailed expressions of $\mathbf{M}(\mathbf{q})$, $\mathbf{C}(\mathbf{q}, \dot{\mathbf{q}})$, and $\mathbf{G}(\mathbf{q})$ refer to Ma et al. [40]. The sampling period is 1 ms. According to

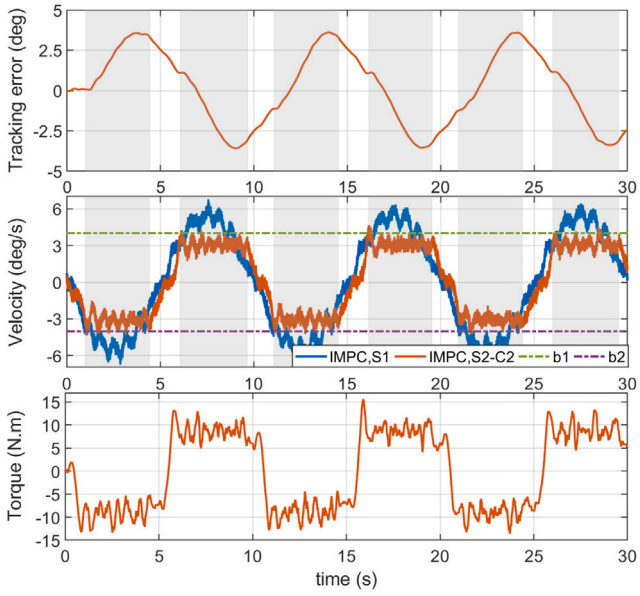

Fig. 10. Exp. results of *S2*: Tracking performance of IMPC with tightened joint velocity constraint, where "b_1" and "b_2" denote the lower and upper bound of joint velocities, "S1" means Scenario 1, and "S2-C2" means Case 2 (C2) in S2. Gray background depicts when the velocity is constrained by control.

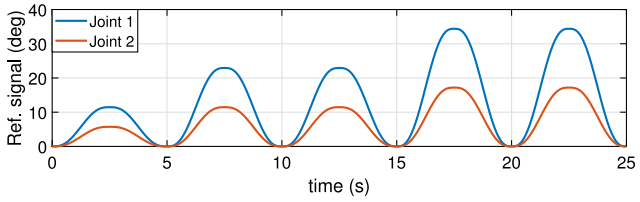

Fig. 11. Reference signals considered for simulations.

procedures in Remark 1, TDE parameters $\bar{\mathbf{M}} = \text{diag}\{0.7, 0.2\}$, $\bar{\mathbf{D}} = \text{diag}\{0.001, 0.001\}$. For the developed IMPC, $\mathbf{Q} = \text{diag}\{3000\mathbf{I}_2, 400\mathbf{I}_2, 300\mathbf{I}_2, 40\mathbf{I}_2\}$, $\mathbf{R} = \mathbf{I}_2$. The `qpOASES` [28] is used to calculate the constrained OCP. The joint position, velocity, and torque limit values are 40 deg, 40 deg/s, and 100 N m, respectively.

In simulations, robustness property of the developed IMPC against modeling errors will be verified, where two groups of simulations are conducted. In the first group (G1), the inertia matrix $\mathbf{M}(\mathbf{q})$ modeling error is considered. There are three situations: (1) $\mathbf{M}(\mathbf{q})$ decreases 50%; (2) $\mathbf{M}(\mathbf{q})$ keeps its nominal value; (3) $\mathbf{M}(\mathbf{q})$ increases 50%. In G1, numerical simulation results of IMPC are also compared with the nonlinear MPC (NMPC) [23] without terminal ingredients, where the following stage cost function is defined:

$$\mathcal{L}'(\mathbf{X}_{k+i+1|k}, \mathbf{u}_{k+i|k}, k) = \|\mathbf{E}_{k+i+1|k}\|^2_{\mathbf{Q}} + \|\mathbf{u}_{k+i|k}\|^2_{\mathbf{R}}. \tag{24}$$

The constrained OCP in the nonlinear MPC scheme is solved by an efficient NLP toolbox, `CasADi` [41], where SQP method is employed.

In the second group (G2), 3 stiffness values (0.9**K**, **K**, 1.1**K**) are considered to verify the developed IMPC still exhibits strong robustness against stiffness uncertainties.

The tracking error is used to measure robustness property of the developed IMPC, and the reference trajectory as shown in Fig. 11 is considered in simulations, where multi-sinusoidal functions are considered.

6.2. Simulation results

The simulation results of G1 are shown in Fig. 12 and Table 2. As shown in Fig. 12 and Table 2, tracking errors are nearly same

Table 2
RMSEs of different controllers (deg), where inertia uncertainties of ±50% are considered.

Method	Joint No.	−50%	Nominal	+50%
IMPC	J1	7.1×10^{-3}	9.6×10^{-3}	1.2×10^{-2}
NMPC	J1	2.4×10^{-1}	4.9×10^{-1}	7.7×10^{-1}
IMPC	J2	6.5×10^{-3}	6.8×10^{-3}	8.8×10^{-2}
NMPC	J2	1.6×10^{-1}	3.1×10^{-1}	4.8×10^{-1}

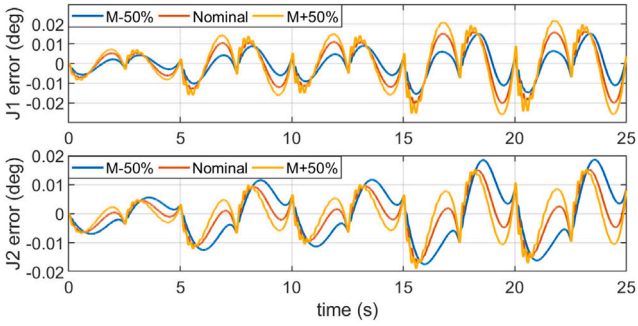

Fig. 12. Simulation results of *G1*: Tracking performance of IMPC with different inertia matrices.

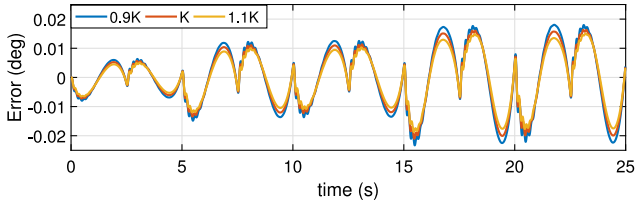

Fig. 13. Simulation results of *G2*: Tracking performance of IMPC with stiffness variations (taking Joint 1 for example).

under inertia matrix uncertainties. This is mainly due to the fact that the inertia modeling error in IMPC is effectively compensated by its time-delay values. The tracking error of NMPC is much higher than that of IMPC, even when the inertial matrix is known exactly. On the one hand, IMPC exhibits strong robustness against inertia modeling errors. On the other hand, due to the reference control signal cannot be determined priorly. Thus, as analyzed in Remark 6, a standard tracking MPC scheme cannot be constructed in NMPC. Normally due to the gravity effects, the non-zero controller is required to maintain the configuration. Since the weighting matrices are constant, we cannot scale the term $\|\mathbf{u}_{k+j|k}\|^2_{\mathbf{Q}}$ to be roughly the same size to the tracking error term $\|\mathbf{E}_{k+j|k}\|^2_{\mathbf{Q}}$. As a result, the tracking error of NMPC is much higher than that of IMPC even when uncertainties do not exist. In addition, the average computing time for IMPC and NMPC at each iteration are 0.63 ms and 3.72 ms, respectively. It further verifies computational efficient property of IMPC.

From Fig. 12, one also learns that with the rise of the amplitude of reference signals, the tracking error increases. When the amplitude of reference signals increases, the operation frequency exhibits a corresponding increase. When the system operates at high frequencies, the TDE error increases and tracking performance will be affected. The simulation results of G2 are shown in Fig. 13. One also observes that tracking performance is also not sensitive to stiffness variations. Different from the state-of-the-art controllers, the stiffness matrix is not required to be known exactly. This is also because the stiffness modeling error is compensated by its time-delay value, which is consistent with the theoretical analysis in Remark 4.

7. Conclusion

This paper introduces a new incremental model predictive controller for a flexible-joint robot. Using the time-delay estimation, the nonlinear dynamics model is approximated by an incremental model, where the joint compliant torque is considered as an intermediate control variable. Then, the incremental model predictive controller is proposed through constructing a constrained optimal control problem, where state predictions are generated by the developed incremental system. Finally, a series of real-time experiments are conducted on the flexible-joint robot and the superior performance of the proposed controller regarding high accuracy, optimality, high computational efficiency and constraint admissibility is demonstrated.

Future work will be devoted to studying IMPC with strict state constraints and less tracking errors, for example, by introducing the Tube-based MPC technique.

CRediT authorship contribution statement

Yongchao Wang: Writing – review & editing, Writing – original draft, Methodology. **Tian Zheng:** Software, Data curation. **Maged Iskandar:** Software. **Marion Leibold:** Methodology. **Jinoh Lee:** Writing – review & editing, Supervision.

Declaration of competing interest

The authors declare that they have no known competing financial interests or personal relationships that could have appeared to influence the work reported in this paper.

Acknowledgments

The authors would like to thank Prof. Martin Buss with the Chair of Automatic Control Engineering (LSR), Technical University of Munich for insightful discussions. We also thank Matthias Kreiner from the Institute of Robotics and Mechatronics, German Aerospace Center (DLR), for the support with experiments.

Data availability

The data that has been used is confidential.

References

[1] Spong MW. An historical perspective on the control of robotics manipulators. Annu Rev Control Robot Auton Syst 2022;5:1–31.
[2] De Luca A, Book WJ. Robots with flexible elements. In: Springer handbook of robotics. Springer, 2016, p. 243–82.
[3] Tomei P. A simple PD controller for robots with elastic joints. IEEE Trans Autom Control 1991;36:1208–13.
[4] Luca AD, Siciliano B, Zollo L. PD control with on-line gravity compensation for robots with elastic joints: Theoy and expeiments. Automatica 2005;41(10):1809–19.
[5] Petit F, Daasch A, Albu-Schäffer A. Backstepping control of variable stiffness robots. IEEE Trans Control Syst Technol 2015;23(6):2195–202.
[6] Yeon JS, Park JH. Practical robust conrol for flexible joint robot manipulators. In: Proc. IEEE int. conf. robot. autom.. ICRA, 2008, p. 3377–82.
[7] Rsetam K, Cao Z, Man Z. Design of robust terminal sliding mode control for underactuated flexible joint robot. IEEE Trans Syst Man, Cybern 2022;52(7):4272–85.
[8] Khan RFA, Rsetam K, Cao Z, Man Z. Singularity perturbation-based adaptive integral sliding mode contro for flexible joint robots. IEEE Trans Ind Electron 2023;70(10):10516–25.
[9] Talole SE, Kolhe JP, Phake SB. Extended-state-observer-based control of flexible-joint system with experimental validation. IEEE Trans Ind Electron 2010;57(4):1411–9.
[10] Gao H, Zhou C, Sun C. Neural network control of a two-link flexible robotic manipulator using assumed mode method. IEEE Trans Ind Inf 2019;15:755–65.
[11] Ma H, Zhou Q, Li H, Lu R. Real-time estimation of model parameters and state-of-charge of li-ion batteries in electric vehicles using a new mixed estimation model. IEEE Trans Cybern 2022;52(12):12905–15.
[12] Wang Y, Zhang Z, Li C, Buss M. Adaptive incremental sliding mode control for a robot manipulator. Mechatronics 2022;82:102717.
[13] Jin M, Lee J, Tsagarakis N. Model-free robust adaptive control of humanoid robots with flexible joints. IEEE Trans Ind Electron 2017;64(2):1706–15.
[14] Lee J, Deshpande N, Caldwell DG, Mattos LS. Microscale precision control of a computer-assisted transoral laser microsurger system. IEEE/ASME Trans Mechatronics 2020;25(2):604–15.
[15] Park SH, Lee J, Seo KH, Jin M. Robust link position tracking control for robot manipulators with series elastic actuators using time-delay estimation. In: Proc. int. conf. robot. automa.. ICRA, 2019, p. 3052–8.
[16] Siciliano B, Book WJ. A singular perturbation approach to control of lightweight flexible manipulators. Int J Robot Res 1988;7(4):79–90.
[17] Ott C, Albu-Schäffer A, Hirzinger G. Comparison of adaptive and nonadaptive tracking control laws for a flexible joint manipulator. In: Proc. IEEE/RSJ int. conf. intell. robots syst.. IROS, 2002, p. 2018–24.
[18] Kim J. Two-time scale control of flexible joint robots with an improved slow model. IEEE Trans Ind Electron 2018;65(4):3317–25.
[19] Farrell J, Polycarpou M, Sharma M, Dong W. Command filtered backstepping. IEEE Trans Autom Control 2009;54:1391–5.
[20] Li C, Liu F, Wang Y, Buss M. Concurrent learning-based adaptive control of an uncertain robot manipulator with guaranteed safety and performance. IEEE Trans Syst Man, Cybern 2022;52:3299–313.
[21] Mayne DQ, Rawlings JB, Rao CV, Scokaert POM. Constrained model predictive control: Stability and optimality. Automatica 2000;36(6):789–814.
[22] Iskandar M, Van Ommeren C, Wu X, Albu-Schäffer A, Dietrich A. Model predictive control applied to different time-scale dynamics of flexible joint robots. IEEE Robot Autom Lett 2023;8(2):672–9.
[23] Köhler J, Müller MA, Allgöwer F. Nonlinear reference tracking: An economic model predictive control perspective. IEEE Trans Autom Control 2019;64(1):254–69.
[24] Seo J, Lee S, Lee J, Choi J. Nonaffine helicopter control design and implementation based on a robust explicit nonlinear model predictive control. IEEE Trans Control Syst Technol 2022;30(2):811–8.
[25] Hewing L, Kabzan J, Zeilinger MN. Cautious model predictive control using Gaussian process regression. IEEE Trans Control Syst Technol 2020;28(6):2736–43.
[26] Xu X, Chen H, Lian C, Li D. Learning-based predictive control dor discrete-time nonlinear systems with stochastic disturbances. IEEE Trans Neural Netw Learn Syst 2018;29(12):6202–13.
[27] Manzano JM, Limon D, Munoz D, Calliess JP. Robust learning-based MPC for nonlinear constrained systems. Automatica 2020;117. Art. no. 108948.
[28] Ferreau HJ. qpOASES: A parametric active-set algorithm for quadratic programming. Math Program Comput 2014;6(4):327–63.
[29] Spong MW. Modeling and control of elastic joint robots. J Dyn Syst Meas Control 1987;109(4):310–8.
[30] De Luca A, Lucibello P. A general algorithm for dynamic feedback linearization of robots with elastic joints. In: Proc. int. conf. robot. and automat.. ICRA, vol. 1, 1998, p. 504–10.
[31] Keppler M, Lakatos D, Ott C, Albu-Schäffer A. Elastic structure preserving (ESP) control for compliantly actuated robots. IEEE Trans Robot 2018;34(2):317–35.
[32] Wang Y, Leibold M, Lee J, Ye W, Xie J, Buss M. Incremental model predictive control exploiting time-delay estimation for a robot manipulator. IEEE Trans Control Syst Technol 2022;30(6):2285–300.
[33] Wang Y, Liu Y, Leibold M, Buss M, Lee J. Hierarchical incremental MPC for redundant robots: A robust and singularity-free approach. IEEE Trans Robot 2024;40:2128–48.
[34] Franklin GF, Powell JD, Workman ML. Digital Control of Dynamic Systems. 3rd ed.. Menlo Park, CA: Addison-Wesley; 1998.
[35] Hsia TC, Gao LS. Robot manipulator control using decentralized linear time-invariant time-delayed joint controllers. In: Proc. int. conf. robot. and automat.. ICRA, vol. 1, 1990, p. 2070–5.
[36] Vito D, Natale C, Antonelli G. A comparison of damped least squares algorithms for inverse kinematics of robot manipulators. IFAC- Pap 2017;50:6869–74.
[37] Albu-Schäffer A, Haddadin S, Ott C, Stemmer A, Wimbock T, Hirzinger G. The DLR lightweight robot: Design and control concepts for robots in human environments. Ind Robot 2007;34(5):376–85.
[38] Loeffl F, Werner A, Lakatos D, Reinecke J, Wolf S, Burger R, Gumpert T, Schmidt F, Ott C, Grebenstein M, et al. The DLR C-runner: Concept, design and experiments. In: Proc. IEEE-RAS 16th int. conf. humanoid robots. 2016, p. 758–65.

[39] Manuel K, Raschel C, Wandinger D, Stemmer A, Ott C. Robust stabilization of elastic joint robots by ESP and PID control: Theory and experiments. IEEE Robot Autom Lett 2022;7:8283–90.

[40] Ma H, Ren H, Zhou Q, Li H, Wang Z. Observer-based neural control of *n*-link flexiblr-joint robots. IEEE Trans Neural Netw Learn Syst 2024;35:5295–305.

[41] Andersson J, Gillis J, Horn G, Rawlings J, Diehl M. CasADi-a software framework for nonlinear optimization and optimal control. Math Program Comput 2019;11:1–36.